JOURNAL OF AIRCRAFT
Vol. 32, No. 1, January–February 1995

Response of a Nonrotating Rotor Blade to Lateral Turbulence Part I: Theory

D. M. Tang* and E. H. Dowell†
Duke University, Durham, North Carolina 27706

Theoretical simulation of a rotor blade in forward flight by a nonrotating rotor blade in a longitudinal sinusoidal pulsating flow, and the flapping and torsional response of a flexible nonrotating rotor blade model to lateral turbulence have been investigated. A direct time domain computational method using a modified linear ONERA aerodynamic model and a time-frequency approach using the classical aerodynamic model have been proposed. A theoretical lift comparison between the classical aerodynamic theory and the modified ONERA model is made. The numerical calculations indicate that the statistically quantitative agreement for both flap and torsional variance responses between the linear ONERA and classical aerodynamic models is reasonably good. The effects of random parametric excitation (when the longitudinal flow includes a turbulence component) and parameter variations are discussed. The numerical results are used to confirm the validity of a new experimental method presented as a companion paper, Part II.

Nomenclature

a_{0l} = blade section linear lift curve slope
$a.c$ = aerodynamic centers of the blade section
b, $\bar{b}$ = blade semichord, b/R
C_l = section lift coefficients
C_m = section pitching moment coefficient
dF_w = section aerodynamic flap component force
dM_x = section aerodynamic pitching moment about the elastic axis
dM_0 = section aerodynamic pitching moment about one-quarter chord
E = modulus of elasticity
e = mass centroid of blade section from the elastic axis
$e.c$ = elastic centers of the blade section
G = shear modulus
g = gravitational acceleration
I = flap area moments
J = torsional stiffness constant
K_m = blade mass radius of gyration
$K_{\phi s}$ = linear torsional spring constant
k = reduced frequency, $b\omega/u_0$
m = mass per unit length of the blade
mc = mass center of the blade section
N = total number of structural modes
NN = number of aerodynamic elements
R = rotor radius
t_τ = b/u_0
U = resultant longitudinal flow velocity, Eq. (6)
u_c, u_s = longitudinal cosine and sine pulsating velocity components
u_G = longitudinal gust velocity, Eq. (1)
u_η = longitudinal turbulence velocity component
u_0 = constant freestream velocity
W_j = generalized coordinates for bending
w = flap bending deflection, perpendicular to v
w_G = resultant lateral gust velocity, Eq. (2)
w_s = lateral sine gust velocity component
w_t = flap deflection at the blade tip
w_γ = lateral turbulence velocity component
x = position coordinate along blade span
α = blade section angle of attack
α_G = gust angle of attack
$\Gamma_{l\gamma}$ = linear circulatory lift of lth aerodynamic section
Δ_l = dimensionless width of lth aerodynamic section
θ_0 = initial pitch angle
ρ = air density
σ_w^2 = variance of flapping response
σ_ϕ^2 = variance of torsional response
τ = reduced time, tU/b
Φ_j = generalized coordinates for torsion
ϕ = twist about deformed elastic axis
ϕ_λ = inflow angle
ω_{xj}, ω_{zj} = jth torsional, flap natural frequency of blade
$(\,)'$ = d( )/dx
$(\dot{\ })$ = d( )/dt

Received Aug. 31, 1993; revision received Feb. 18, 1994; accepted for publication May 3, 1994.

*Research Associate, Department of Mechanical Engineering and Materials Science.
†Dean, School of Engineering. Department of Mechanical Engineering and Materials Science.

I. Introduction

HELICOPTER response to atmospheric turbulence excitation is important because it not only affects ride quality, but also contributes to structural fatigue, especially for hingeless configuration helicopters that have higher dynamic stresses and vibration levels. Recently, increased attention has been given to turbulence modeling and related effects on helicopter response. Two atmospheric turbulence models are often used to analyze gust response. They are the body-fixed sampling model that refers to the actual atmospheric turbulence experienced by a point fixed on the rotor hub, and the blade-fixed sampling model that refers to the atmospheric turbulence experienced by an element of the rotating rotor blade. Recent studies[1,14,15] show that the gust velocity environments of the rotor hub and the blade tip are substantially different. Rotational velocity effects are dominant for a conventional helicopter, particularly for low-advance ratio ($\mu < 0.4$) and low-altitude flight. Therefore, the blade-fixed sampling model is theoretically more accurate for defining the gust velocity field.

However, whatever turbulence sampling models are used, the calculation of the covariance of blade response to a gust or atmospheric turbulence can be classified as a parametric random vibration. The mathematical model of a rotor blade response in forward flight is described by a set of coupled equations of motion with time-dependent coefficients. This is because the flowfield relative to the rotating blade provides

certain aerodynamic damping and spring forces acting on the blade that are changing periodically or randomly with time. The generalized aerodynamic forces that appear as inhomogeneous terms on the right sides of the equations are the result of a random process modulated by a deterministic periodic function generated by the rotating blade. Even if the atmospheric turbulence excitation is a stationary stochastic process, the actual forces acting on the rotor blade are part of a near cyclostationary process.

Theoretical computation of the response covariance matrix of the rotor blade has been obtained by many approximate methods for solving the parametric random vibration problem. The most insightful gust response analysis has been conducted by Bir and Chopra.[3] They considered a coupled rotor/fuselage system with a complete coupled flap-lag-torsional blade model. The response analysis is similar to the approach for a fixed wing aircraft using the general finite element method. A three-dimensional gust excitation with step, sine-squared gust profiles in a body-fixed sampling model was used. In Refs. 4–9 the effect of random air turbulence on blade stability and response in hover and in forward flight was studied using modern stochastic methods. The parametric random vibration equations were converted to *Itô*-type stochastic differential equations that were then used to determine the stochastic stability and statistical moments of the response. The turbulence is assumed to be a "filtered" white noise or a strictly white noise using the body-fixed sampling model. In Refs. 10–13 a mixed time-frequency domain method was proposed for the high advance ratio case. In these methods, both the numerical time integration and frequency domain solution are used to determine the statistical quantities of the response. In Ref. 14 a direct time domain approach was developed. The statistically meaningful characteristics of the response (covariance and correlation) are directly obtained from a pair of ordinary matrix differential equations in the time domain. This method is attractive in that the relevant algorithm is simple and efficient. A frequency-time spectrum method that simultaneously predicts both frequency and temporal characteristics,[1,15] and a new time-domain method for simulating cyclostationary turbulence[2] using the blade-fixed sampling model, were proposed for low altitudes and low speed in forward flight. However, the computational costs are high when the number of degrees of freedom (DOF) of rotor system increases.

In this article, a mathematical model for computing the response of a nonrotating rotor blade to a lateral turbulence in a sinusoidal pulsating flow, i.e., a gust response to deterministic and random parametric excitations, is pursued. It is found that the differential equations that describe the above problem are similar to those for the gust response of a helicopter rotor blade to lateral turbulence in forward flight. The aerodynamic effects due to the rotating speed relative to the blade are simulated by a special flowfield with a sinusoidal pulsating stream and lateral turbulence. We assume the atmospheric turbulence to be homogeneous and isotropic, and the effects of self-induced turbulence by the lifting surface, such as downwash and trailing vortices, to be negligible. The response statistics vs azimuth angle of the rotor blade are determined by a controllable field parameter. This simulation relative to an actual helicopter rotor is incomplete because the centrifugal and Coriolis effects due to the rotating speed of the rotor blade are not considered in the experimental model. However, the latter are readily incorporated into the theoretical model, and in an experimental study such effects could be corrected for theoretically (see Part II).

For this mathematical model a time-frequency domain computational method[10-13] based on the classical aerodynamic theory is used to predict the gust response of a rotor blade to cyclostationary turbulence excitation. This method is based on the concept of an equivalent energy, i.e., the mean square response to a random excitation is equal to that due to a periodic function excitation at the resonant frequencies of this system. Therefore, a random response problem is transformed to an equivalent deterministic problem. A comparison with a conventional time-domain method based on the linear ONERA aerodynamic model is also made. In order to determine the ONERA model coefficients for the sinusoidal pulsating flow, a theoretical lift comparison between the classical aerodynamic theory and the modified ONERA model is made. The numerical calculations indicate that the statistically quantitative agreement for both flap and torsional variance responses between the linear ONERA and classical aerodynamic models is reasonably good. The effects of random parametric excitation (when the longitudinal flow includes a small turbulence component) and parameter variations are discussed. The numerical results are compared with the experimental data in Part II.[24]

II. Equations of Motion of Flexible Blade

A vertical, nonrotating elastic cantilevered blade model with flap-torsional coupling and a pitch spring constraint at the root is used. The linear equations of motion may be written as

$$EIw'''' + m\ddot{w} + me\ddot{\phi} + w_{mg} = \frac{dF_w}{dx} \tag{1}$$

$$-GJ\phi'' + mK_m^2\ddot{\phi} + me\ddot{w} + M_k = \frac{dM_x}{dx} \tag{2}$$

Note that ϕ is measured with respect to the deformed elastic axis. For the blade structure with a pitch spring at the root, the torsional motion ϕ includes elastic torsional deformation along the blade span and pitch motion at the blade root.

The gravitational elastic potential energy of the blade is

$$V_{mg} = -\frac{1}{2} mg \int_0^R \int_0^x (w')^2 \, dx \, dx$$

and the potential energy from the root spring motion is

$$V_k = \frac{1}{2} K_\phi [\phi(0, t)]^2$$

From V_{mg} and V_k the restoring stiffness terms w_{mg} and M_k may be deduced by variational methods.

A. Specific Gust Flowfield

In order to simulate the parametric random vibration motion of a rotor blade in forward flight (i.e., a differential equations of motion simulation rather than a physical simulation of a practical rotorcraft), the gust flowfield environment is especially designed. A dominant lateral turbulence velocity component and also a lateral sinusoidal component with a rotor speed frequency Ω that are both normal to the blade plane are considered. The turbulence for the present study is homogeneous and isotropic over the whole span of the blade model, and has a sufficiently large component of uniform power spectral density over the fundamental blade response frequency band. Also, a dominant longitudinal sinusoidal component with a rotor speed frequency and a longitudinal turbulence velocity component that are parallel to the blade plane are considered.

The longitudinal and lateral gust velocities are given by

$$u_G = u_s \sin \Omega t + u_\eta \tag{3}$$

$$w_G = w_s \sin \Omega t + w_\gamma \tag{4}$$

Physically, the longitudinal gust is a sinusoidal pulsating stream (when $\mu_\eta = 0$). The aerodynamic forces are similar to those forces produced by a rotating blade in forward flight.

Since the freestream includes sinusoidal pulsating components, the aerodynamic forces generated by w_G are modulated by sin Ωt. These forces have cyclostationary characteristics.

For u_η, if the power spectral density of u_η is known, e.g., $S_u(\omega)$, we can use Shinozuka's algorithm[17] to express the turbulence process as a pseudoperiodic series, i.e.,

$$u_\eta(t) = 2\sum_{i=1}^{N}\sqrt{S_u(\omega_i)\Delta\omega}\cos(\omega_i t + \Phi_i) \tag{5}$$

where $\omega_i = (2i - 1)\Delta\omega/2$ and $\Delta\omega$ and Φ_i are subdivisions of the power spectral density and the phase of the ith spectral component, respectively. Φ_i is treated as a random variable with uniformly distributed probability density between 0 and 2π. In the above equation, only the positive spectral components S_u, and frequencies ω_i, are used. The essence of this approximation is to replace the random function $u_\eta(t)$ by an equivalent periodic function.

The Fourier transform of the random longitudinal velocity is

$$u_{\eta f}(\omega) = \frac{1}{2\pi}\int_{-\infty}^{\infty} u_\eta(t)e^{-i\omega t}\,dt \tag{6}$$

Taking a finite number of terms in the Fourier series, one obtains

$$u_\eta(t) \approx \sum_{i=1}^{N}[u_{\eta ci}(\omega_i)\cos\omega_i t + u_{\eta si}(\omega_i)\sin\omega_i t] \tag{7}$$

and the resultant longitudinal velocity is represented as

$$U = u_0 + u_s \sin\Omega t + u_\eta$$

where $u_{\eta ci}(\omega_i)$ and $u_{\eta si}(\omega_i)$ are the real and imaginary components of the Fourier transform, which may be determined in terms of the power spectra density $S_u(\omega)$ of the random function. $u_s \sin\Omega t$ is used to simulate the rotational speed of the blade.

For w_γ, the same procedure is used.

Two aerodynamic models of incompressible two-dimensional flow are considered for dealing with the time-frequency solution and direct time domain solution of the blade response, respectively. These are considered next.

B. Classical Aerodynamic Model

In Ref. 16, the force and moment acting on a two-dimensional airfoil executing harmonic motion in a sinusoidal pulsating stream are derived on the basis of nonstationary incompressible potential-flow theory, with the inclusion of the effect of the continuous sheet of vortices shed from the trailing edge. Also, the classical Sears gust response theory is included in this model. A sketch of the two-dimensional airfoil is shown in Fig. 1. The total force on the blade per span is given by

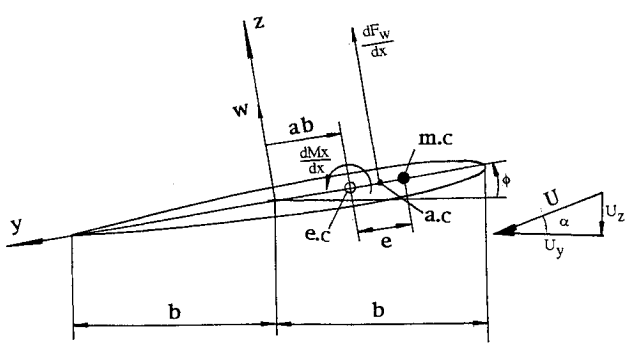

Fig. 1 Sketch of the two-dimensional airfoil.

$$\frac{dF_w}{dx} = \pi\rho b^2[\ddot{w} + U\dot{\phi} + \dot{U}(\phi + \theta_0) - ab\ddot{\phi}] + 2\pi\rho U\{(u_0 + u_{r1})\theta_0 + [b(0.5 - a)\dot{\phi} + u_0\phi]C(k) + \dot{w}C(k) + u_{r2}\phi\} + \pi\rho bUu_0S(k)\alpha_G \tag{8}$$

and the total moment about the point at elastic center of the blade is

$$\frac{dM_x}{dx} = \pi\rho b^2[Ub(0.5 - a)\dot{\phi} - \dot{U}ba(\phi + \theta_0) - ba\ddot{w} + b^2(0.125 + a^2)\ddot{\phi}] + 2\pi\rho Ub^2(a + 0.5)\{(u_0 + u_{r1})\theta_0 + [b(0.5 - a)\dot{\phi} + u_0\phi]C(k) + \dot{w}C(k) + u_{r2}\phi\} - b(0.5 + a)2\pi\rho bUu_0S(k)\alpha_G \tag{9}$$

where

$$u_{r1} = u_sC(k_\Omega)\sin\Omega t + \sum_{i=1}^{N}C(k_{\omega i})(u_{\eta ci}\cos\omega_i t + u_{\eta si}\sin\omega_i t)$$

$$u_{r2} = u_sC(k_\Omega)\sin\Omega t + \sum_{i=1}^{N}C(k_{\omega i+\Omega})(u_{\eta ci}\cos\omega_i t + u_{\eta si}\sin\omega_i t)$$

and $k_\Omega = \Omega b/u_0$, $k = \omega b/u_0$, $k_{\omega i} = \omega_i b/u_0$, $k_{\omega i+\Omega} = (\Omega + \omega_i)b/u_0$, $S(k)$ is Sears' coefficient, and $C(k)$ is Theodorsen's coefficient, see Ref. 21, pp. 409–412.

C. Linear ONERA Aerodynamic Model

The semiempirical ONERA model is derived using measured wind-tunnel data for an oscillating airfoil in conjunction with a parameter identification scheme as shown in Ref. 18. The lift and moment coefficients of each blade section in the differential equations are described in terms of a reduced time. A differential operator relative to the real time d/dt is used in this article for comparison with the experimental data.

Comparing the Greenberg theory to the original ONERA model,[18] we find that the apparent mass term $\dot{U}\alpha$ induced by unsteady pulsating stream is not accounted for in the latter model. It is also noted that the pulsating stream directly affects circulation rather than the lift coefficient. Therefore, we must write a circulation equation (not a lift coefficient equation) for the pulsating stream case. Reference 19 proposed a modified ONERA aerodynamic model in a circulation equation form. It is suitable for the present study. The relevant linear ONERA equations are

$$L = L_{l0} + \rho bU_y\Gamma_{l\gamma} \tag{10}$$

$$L_{l0} = \pi\rho bs_lt_TU\dot{U}_z \tag{11}$$

$$t_\tau\dot{\Gamma}_{l\gamma} + \lambda_l\Gamma_{l\gamma} = \lambda_la_{0l}U_z + t_\tau\delta_lU\dot{\varepsilon} \tag{12}$$

where

$$\alpha = \phi + \theta_0 + \alpha_G - \phi_\lambda, \qquad \alpha_G = w_{G_T}/u_0$$

$$\phi_\lambda \approx \dot{w}/u_0, \qquad U_y = U\cos\alpha \approx U$$

$$U_z = U\sin\alpha \approx U\alpha, \qquad \dot{U}_z = \dot{U}\alpha + U\dot{\alpha}$$

$\dot{\varepsilon}$ is the rate of rotation of the airfoil with respect to the air mass, and here, it is assumed that $\dot{\varepsilon} \cong \dot{\phi}$.

For the aerodynamic coefficients in a constant longitudinal flow, e.g., s_l, a_{0l}, δ_l, and λ_l, of the NACA 0012 airfoil, see the next section.

For the moment equation, we also obtain a set of equations similar to Eqs. (10–12). The corresponding coefficients are $\Gamma_{m\gamma}$, s_m, λ_m, c_m, and δ_m. The moment is taken about the rotor blade quarterchord. L_{l0}, M_0 [see Eq. (11)] are the noncirculatory lift and moment components due to the effect of the air apparent mass. $\Gamma_{l\gamma}$, $\Gamma_{m\gamma}$ [see Eq. (12)] are the linear circulatory lift and moment aerodynamic components associated with the unsteady freestream. For the NACA 0012 airfoil, $c_m = 0$ and $\lambda_m = 0$ (see Ref. 20), $\Gamma_{m\gamma}$ is assumed to be zero, and

$$M = M_0 = 2\rho b^2 t_r s_m U \dot{U}_z$$

where $s_m = -(\pi/4)(\text{rad}^{-1})$

The ONERA aerodynamic model is based on a blade airfoil element. Here, it is applied to a flexible blade motion problem. A simple assumption is that the blade is divided into several spanwise aerodynamic sections, e.g., *NN*, and the ONERA model is applied to each section. For the *l*th blade section, the variables $\Gamma_{l\gamma}$, and α_G, ϕ, w should have a subscript l in these equations:

$$\frac{dF_w}{dx} = L \tag{13}$$

$$\frac{dM_x}{dx} = M + b(0.5 + a)L \tag{14}$$

D. Lift Comparison Between the Two Aerodynamic Models

There are no experimental data λ_l for the NACA 0012 airfoil in the present pulsating flow case. Therefore, numerical lift comparisons between the two aerodynamic models have been made. The experimental data in the absence of sinusoidal pulsating flow suggest $a_{0l} = 5.9$, $\lambda_l = 0.15$, $\delta_l = 3.245$, and $s_l = 5.16$ for the NACA 0012 airfoil. The structural plunge w and pitch angle ϕ are assumed to be zero, and the initial pitch angle of this airfoil θ_0 to be 3 deg. The unsteady freestream is expressed as

$$U = u_0(1 + \mu \sin \Omega t)$$

Figure 2 shows the time history of the lift ratio, $|L/L_0|$, ($L_0 = \rho b a_{0l}\theta_0 u_0^2$) for $\Omega = 5$ Hz, $\mu = 0.1$, and $k_\Omega = 0.062$. The solid line denotes the result from the classical aerodynamic model. The dashed line and symbol ○ denote the results from the ONERA model with $\lambda_l = 0.15$ and $\lambda_l = 0.3$ (assumed) for the NACA 0012 airfoil, respectively. It is found that the motions are sinusoidal for both aerodynamic models, and the lift amplitude difference between the two models is very small, and the effect of the time delay parameter λ_l can be negligible. When μ increases, the lift difference still is small (it is not shown). This is because at small reduced frequency k_Ω the two aerodynamic models are basically identical. When k_Ω increases, e.g., $k_\Omega = 0.3$, the lift amplitudes are different as shown in Fig. 3a for $\mu = 0.1$, and Fig. 3b for $\mu = 0.5$. The difference between two aerodynamic models decreases as λ_l increases from 0.15 to 0.3, and as μ = decreases from 0.5 to 0.1. Recall that for sinusoidal airfoil motion in a pulsating stream, we can obtain a lift coefficient $C_l(k_\Omega)$ similar to the Theodorsen function $C(k_\Omega)$. It is given by

$$C_l(k_\Omega) = \frac{\lambda_l^2}{\lambda_l^2 + k_\Omega^2} + i\frac{\lambda_l k_\Omega}{\lambda_l^2 + k_\Omega^2}$$

where $C_l(k_\Omega)$ depends on the reduced frequency k_Ω as well as λ_l.

Figures 4 and 5 show the average lift ratio $|L/L_0|_{ave}$, and the rms lift ratio, $|L/L_0|_{rms}$, vs k_Ω for $u_0 = 20$ m/s, $\mu = 0.1$ and, $\lambda_l = 0.15$ and $\lambda_l = 0.3$ (assumed) for an NACA 0012 airfoil as obtained from the ONERA model and the classical aerodynamic model. The solid line denotes the result from the classical aerodynamic model. The dashed line and symbol ○ denote the results from the ONERA model with $\lambda_l = 0.15$

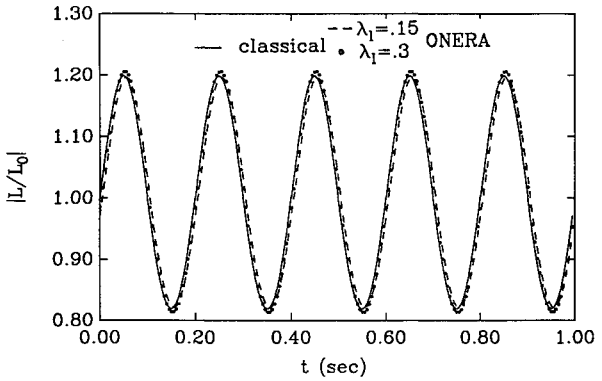

Fig. 2 Time history of lift ratio $|L/L_0|$ for $\Omega = 5$ Hz, $k_\Omega = 0.0628$ and $\mu = 0.1$: —, classical model; - -, ONERA model $\lambda_l = 0.15$; ○, ONERA model $\lambda_l = 0.3$.

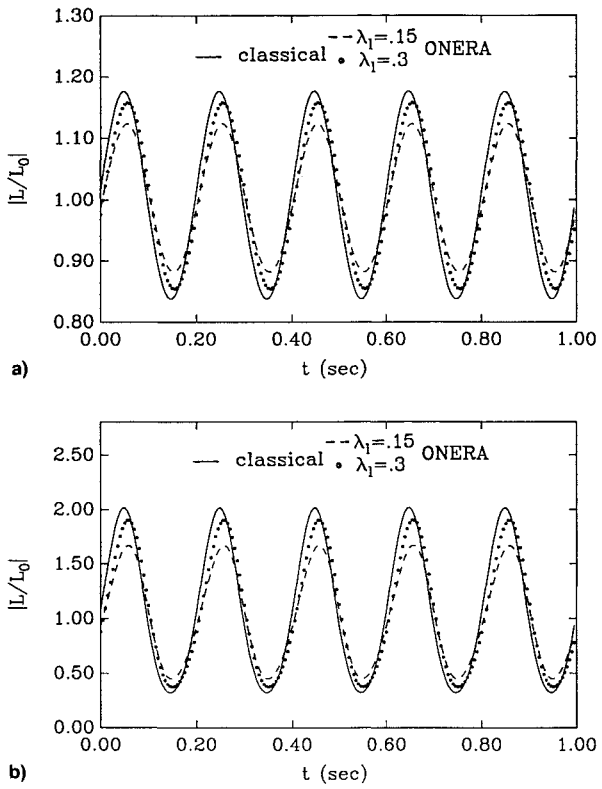

Fig. 3 Time history of lift ratio $|L/L_0|$ for $\Omega = 5$ Hz and $k_\Omega = 0.3$, —, classical model; - -, ONERA model $\lambda_l = 0.15$; ○, ONERA model $\lambda_l = 0.3$, for a) $\mu = 0.1$ and b) $\mu = 0.5$.

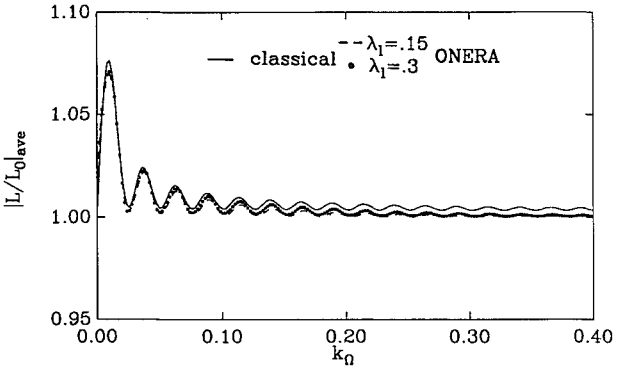

Fig. 4 Average lift ratio vs k_Ω for $u_0 = 20$ m/s, $\mu = 0.1$ and $\lambda_l = 0.15$ and 0.3: —, classical model; - -, ONERA model $\lambda_l = 0.15$; ○, ONERA model $\lambda_l = 0.3$.

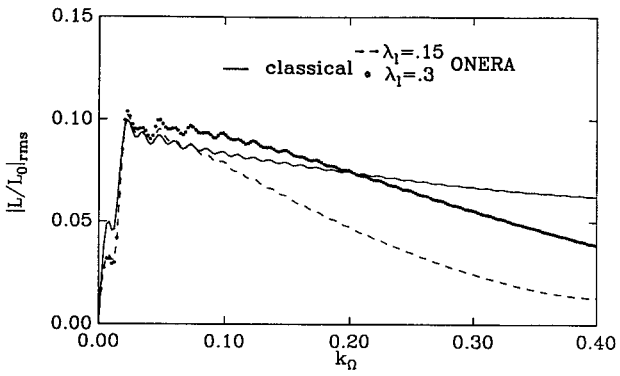

Fig. 5 Root mean square lift ratio vs k_Ω for u_0 = 20 m/s, μ = 0.1 and λ_l = 0.15 and 0.3: —, classical model; - -, ONERA model λ_l = 0.15; ○, ONERA model λ_l = 0.3

and $\lambda_l = 0.3$ (assumed). It is found from Fig. 4 that the average lift is a decaying oscillation curve for both models, and as k_Ω increases, the response from the ONERA model approaches unity. With respect to the rms responses, the result from the ONERA model for $\lambda_l = 0.3$ is close to that from the classical model, especially in the small reduced frequency range.

For qualitative purposes, we compare results from the ONERA model for different λ_l to the approximations of the Wagner and Küssner functions, given in pp. 344 and 345 of Ref. 21. For pitch (Wagner)

$$\bar{L}(\tau) = 1 - 0.165e^{-0.462\tau} - 0.335e^{-0.3\tau}$$

and for plunge (Küssner)

$$\bar{L}(\tau) = 1 - 0.5e^{-0.13\tau} - 0.5e^{-\tau}$$

Now for the ONERA model following Ref. 19, for pitch (including the δ_l term)

$$\bar{L}(\tau) = 1 - [(a_{0l} - \delta_l/a_{0l})e^{-\lambda_l\tau}$$

and for plunge (no δ_l term)

$$\bar{L}(\tau) = 1 - e^{-\lambda_l\tau}$$

where τ is reduced time.

A comparison of the ONERA results for the NACA 0012 airfoil and the Wagner-Küssner results is given in Figs. 6a and 6b for λ_l = 0.15, 0.3(δ_l = 0), and λ_l = 0.15, 0.3(δ_l = 3.245), respectively. The dashed and solid lines denote the Wagner and Küssner functions, respectively. The symbols ○ and ⊙ denote the ONERA results of λ_l = 0.15 and λ_l = 0.3 for δ_l = 0 and δ_l = 3.245, respectively. It is found that in the case of δ_l = 3.245, the result for λ_l = 0.15 is very close to the Wagner function, and the difference between the curves for λ_l = 0.15 and λ_l = 0.3 is small as shown in Fig. 6a. However, for δ_l = 0, the difference is larger as shown in Fig. 6b. It is thought that λ_l = 0.3 may be a better approximate value for the unsteady freestream case in the present ONERA model.

E. Equations of Motion with the Classical Aerodynamic Model

In Eqs. (1) and (2), expansions in general mode shape functions are used to obtain ordinary differential equations in terms of generalized modal coordinates. They are expressed in series form as follows:

$$\bar{w} = \sum_{j=1}^{N} W_j(t)\psi_j(\bar{x})$$
$$\phi = \sum_{j=1}^{N} \Phi_j(t)\Theta_j(\bar{x}) \tag{15}$$

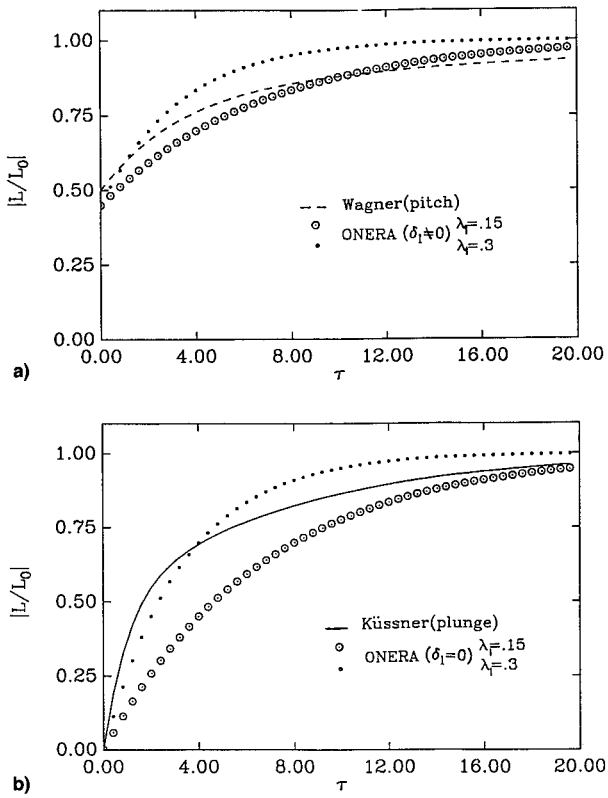

Fig. 6 Lift ratio vs τ for λ_l = 0.15 and 0.3, for a) Wagner (pitch) theory and b) Küssner (plunge) theory.

where $(\bar{})$ indicates nondimensionalization of the spanwise coordinate with respect to the blade span R, and ψ_j, Θ_j, λ_j, σ_j, and γ_j are the characteristic functions for nonrotating cantilevered beam vibrations.

Substituting Eqs. (8), (9), and (15) into Eqs. (1) and (2) and using the Galerkin method, one obtains the modal matrix equations of motion in second-order form. They are given by

$$[M]\{\ddot{q}\} + \frac{U}{R}[C]\{\dot{q}\} + \left([K_0] + \frac{\dot{U}}{R}[K_1] + \frac{Uu_{r2}}{R^2}[K_2] + \frac{Uu_0}{R^2}[K_3]\right)\{q\} = \frac{Uu_0}{R^2}\{F_1\}S(k)\alpha_G + \left(\frac{\dot{U}}{R} + \frac{U(u_0 + u_{r1})}{R^2}\right)\{F_1\}\theta_0 \tag{16}$$

where

$$\{q\}^T = \lfloor \ldots W_j \ldots \Phi_j \ldots \rfloor$$

and $[M]$, $[K_0]$, $[K_1]$, and $[K_2]$ are constant matrices that depend upon the structural parameters, see Ref. 22. $[C]$ and $[K_1]$ depend upon Theodorsen's function $C(k)$, as well as the structural and aerodynamic parameters. Equation (16) is a set of parametric random differential equations for a $2N$ degree-of-freedom system.

F. Equations of Motion with the Linear ONERA Aerodynamic Model

Substituting Eqs. (13–15) into Eqs. (1) and (2) and using the Galerkin method, one obtains a set of $2N$ differential equations in terms of generalized coordinates. Substituting Eqs. (11) and (12) into Eq. (10), we obtain NN first-order differential equations for the aerodynamic coefficients, $\Gamma_{ly'}$. Upon introducting a $4N + NN$ state vector $\{q_b\}$, which by

stipulation is identical to the response vector, the blade equation of motion can be expressed as

$$\begin{bmatrix} \hat{M}_{jj} & \hat{M}_{jl} \\ \hat{M}_{lj} & \hat{M}_{ll} \end{bmatrix} \begin{Bmatrix} \dot{q}_{bj} \\ \dot{q}_{bl} \end{Bmatrix} = \begin{bmatrix} \hat{K}_{jj} & \hat{K}_{jl} \\ \hat{K}_{lj} & \hat{K}_{ll} \end{bmatrix} \begin{Bmatrix} q_{bj} \\ q_{bl} \end{Bmatrix} + \begin{Bmatrix} \hat{F}_j \\ \hat{F}_l \end{Bmatrix} (\theta_0 + \alpha_G) \tag{17}$$

where

$$\{q_b\} = \begin{Bmatrix} q_{bj} \\ q_{bl} \end{Bmatrix}$$

$$\{q_{bj}\}^T = \{ \ldots . \dot{W}_j, W_j, \dot{\Phi}_j, \Phi_j \ldots . \}^T$$

$$\{q_{bl}\}^T = \{ \ldots . C_{Tyl} \ldots . \}^T$$

and the submatrices $\hat{M}_{jj}$, $\hat{M}_{ll} \ldots$, $\hat{K}_{jj}$, $\hat{K}_{ll} \ldots$ depend upon the structural parameters and aerodynamic parameters, as well as u_0, u_s, and u_η pulsating stream. It is noted that the term of $\dot{\alpha}_G$ is neglected in Eqs. (16) and (17) for simplicity. This means that the effects of atmospheric turbulence time rate on the fluid apparent mass are neglected.

III. Computation of Blade Random Response

A. Solution by a Time-Frequency Domain Method

The time frequency domain method is used to solve Eq. (16). The solutions of Eq. (16) include the deterministic periodic response generated by the second excitation term due to θ_0 on the right of the equations, and the random response created by the first excitation term due to α_G.

It is assumed that the Fourier transform of α_G exists, i.e., $F_\alpha(\omega)$, which is given by

$$\alpha_G(t) = \int_{-\infty}^{\infty} F_\alpha(\omega) e^{i\omega t} \, d\omega \tag{18}$$

Because of the linear nature of this equation, the particular solution (see Chap. 6 of Ref. 23) can be written as

$$g(t) = \int_{-\infty}^{\infty} F_\alpha(\omega) H(\omega, t) \, d\omega \tag{19}$$

where $H(\omega, t)$ is the complex valued response function to the input of $(Uu_0/R^2)S(k)\{F_1\}e^{i\omega t}$, with zero initial conditions. Following Ref. 11, when the input function is a nonstationary random process with a double frequency power spectral density, the response autocorrelation function is generally expressed as

$$R_q(t_1, t_2) = \int_{-\infty}^{\infty} \int_{-\infty}^{\infty} S_\alpha(\omega_1, \omega_2) H(\omega_1, t_1) H^*(\omega_2, t_2) \, d\omega_1 \, d\omega_2 \tag{20}$$

As mentioned before, α_G is assumed to be a stationary stochastic process, and we have

$$S_\alpha(\omega_1, \omega_2) = S_\alpha(\omega_1)\delta(\omega_2 - \omega_1) \tag{21}$$

where $\delta(\omega)$ is the Dirac delta function.

Substituting Eq. (21) into Eq. (20), one obtains

$$R_q(t_1, t_2) = \int_{-\infty}^{\infty} S_\alpha(\omega) H(\omega, t_1) H^*(\omega, t_2) \, d\omega \tag{22}$$

where $R_q(t_1, t_2)$ is the autocorrelation function of the generalized coordinate q evaluated at t_1 with lag $(t_1 - t_2)$ of the independent time variables t_1 and t_2. For the helicopter blade response, t_1 and t_2 may be regarded as azimuth angles and, after many rotations, each cycle of rotor response may be regarded as one member of an ergodic ensemble, from which the average over a given number of rotations, e.g., M cycles, may be taken.

Setting $t_1 = t_2 = t$, i.e., the lag time is zero, then the time variable variance response is

$$\sigma_q^2(t) = R_q(t, t) = \int_{-\infty}^{\infty} S_\alpha(\omega) H(\omega, t) H^*(\omega, t) \, d\omega \tag{23}$$

or

$$\sigma_q^2(t) = \int_{-\infty}^{\infty} S_\alpha(\omega)[H_c^2(\omega, t) + H_s^2(\omega, t)] \, d\omega \tag{24}$$

where $H_c(\omega, t)$ and $H_s(\omega, t)$ are the frequency response functions due to the inputs of $(Uu_0/R^2)S(k)\{F_1\}\cos \omega t$, and $(Uu_0/R^2)S(k)\{F_1\}\sin \omega t$, respectively.

Now, $S_\alpha(\omega, t)$ is divided over the positive frequency range into M intervals, $\Delta\omega = \omega_{\max}/M$, where $\omega_{\max}$ is the maximum frequency considered. The newly constructed power spectral density (PSD) is given by

$$\int_0^{\infty} S_\alpha(\omega, t) \, d\omega = 2 \sum_{i=1}^{M} \sigma_{\alpha i}^2(\omega, t)\delta(\omega - \omega_i) \tag{25}$$

Selecting in each interval a central frequency ω_i, and multiplying $\delta(\omega - \omega_i)$ with the integral of $S_\alpha(\omega, t)$ over this interval, the variance of the ith portion of the $S_\alpha(\omega, t)$ is given by

$$\sigma_{\alpha i}^2(\omega, t) = \int_{\omega_i - \Delta/2}^{\omega_i + \Delta/2} \Phi(\omega, t) \, d\omega \tag{26}$$

Finally, an approximate expression for the time variable variance is given by

$$\sigma_{qq}^2(t) = 2 \sum_{i=1}^{M} [H_c^2(\omega_i, t) + H_s^2(\omega_i, t)]\sigma_{\alpha i}^2(\omega_i, t) \tag{27}$$

and the time variable variance of the response rate is

$$\sigma_{\dot{q}\dot{q}}^2(q) = 2 \sum_{i=1}^{M} [\dot{H}_c^2(\omega_i, t) + \dot{H}_s^2(\omega_i, t)]\sigma_{\alpha i}^2(\omega_i, t) \tag{28}$$

and the time variable cross variance between the response and response rate is

$$\sigma_{qq}^2(t) = 2 \sum_{i=1}^{M} [H_c(\omega_i, t)\dot{H}_c(\omega_i, t) + H_s(\omega_i, t)]\sigma_{\alpha i}^2(\omega_i, t) \tag{29}$$

B. Solution by a Time-Domain Method

For Eq. (17), a direct time domain solution can be obtained. Because the time histories of the gust angle α_G and the pulsating stream U are known from the theory or from the experiment, the gust response can be determined by numerical time integration. The variance responses in flap σ_w^2 and twist σ_ϕ^2 are obtained using a general statistical analysis method for the response time histories.

IV. Numerical Examples

A numerical simulation of the statistical response of a nonrotating blade model to atmospheric turbulence in an unsteady freestream has been made. The model parameters are listed in Table 1. The theoretical results are obtained by taking three modes for the flapwise deflection and two modes for the twist. The response results are expressed as a variance at the tip of the blade. For the time domain method, the blade is divided into four equal length aerodynamic elements. The

Table 1 Model parameters

R	19.68, in.
b	1.57, in.
ω_z	10, Hz
ω_x	17.8, Hz
GJ	0.25×10^4, lb/in.^{2}
m	0.47×10^{-4}, lb^2/in.^{2}
K_m	1.149, in.
$K_{\phi s}$	18.62, lb/in./rad
e	0.315, in.
ab	−0.63, in.

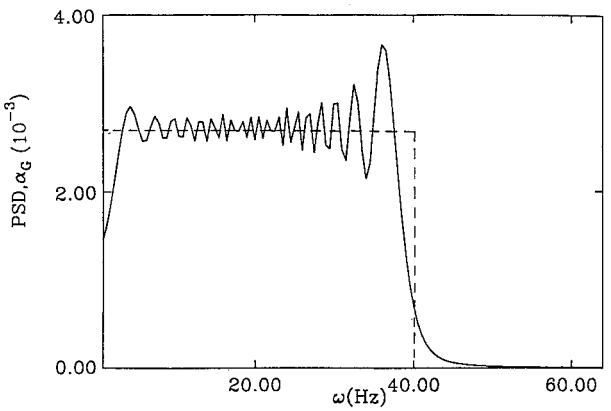

Fig. 7 Theoretical lateral gust PSD.

turbulence has a uniform power spectral density over 0–40-Hz frequency band. The PSD of the gust angle of attack α_G is 0.0027 (deg)^2/Hz as shown by an approximate curve (dashed line) in Fig. 7. The solid line is generated by a frequency sweep function. For the time-frequency method, the PSD curve is divided into 40 intervals and $\Delta\omega = 1$ Hz.

In the numerical examples, "turbulence" in a pulsating stream as generated by a frequency sweep signal is also considered. The amplitude is 0.02 u_0, and the PSD of u_η is similar to the one for α_G from 0–40 Hz.

A. Nonrandom Parametric Excitation

In this case, the longitudinal turbulence velocity is negligible, i.e., u_η is taken as zero.

Figures 8a and 8b show a comparison of results from the time-frequency method and direct time domain method, or correspondingly the results obtained from the classical aerodynamic model and the linear modified ONERA model for $\theta_0 = 0$, $u_0 = 23$ m/s, $\mu = 0.1$, $\Omega = 8$ Hz, and "one cycle" of rotor blade motion. In fact, the blade does not rotate, but the oncoming flow relative to the fixed blade is a sinusoidal pulsating stream with a oscillation frequency 8 Hz, therefore one cycle is equal to 1/8 s, or as presented here is 2π corresponding to the azimuth angle of the rotating blade. In the direct time domain method, the integration step length is taken as 1/800 s, and the total integration time is 15 s or 12,000 points. The variance of the flap and torsional responses are statistically determined from 12,000 points of response data. The solid and dashed lines denote the results from time-frequency and direct time domain methods, respectively. The quantitative agreement is reasonably good and the motions appear to be periodic for both flapwise and torsional variance responses. However, the results from time-frequency method appear closer to a pure single harmonic motion than those from direct time integration. The latter has more harmonic response components. The flap and torsional variance responses have about two and four response peaks, because the rotor speed frequency $\Omega = 8$ Hz, is near the first flap natural frequency ($\omega_z = 10$ Hz), and about half the first torsional natural frequency ($\omega_x = 17$ Hz).

Figures 9a and 9b show the time-varying variance responses of the flap motion for several different μ and $\theta_0 = 0$, $u_0 =$

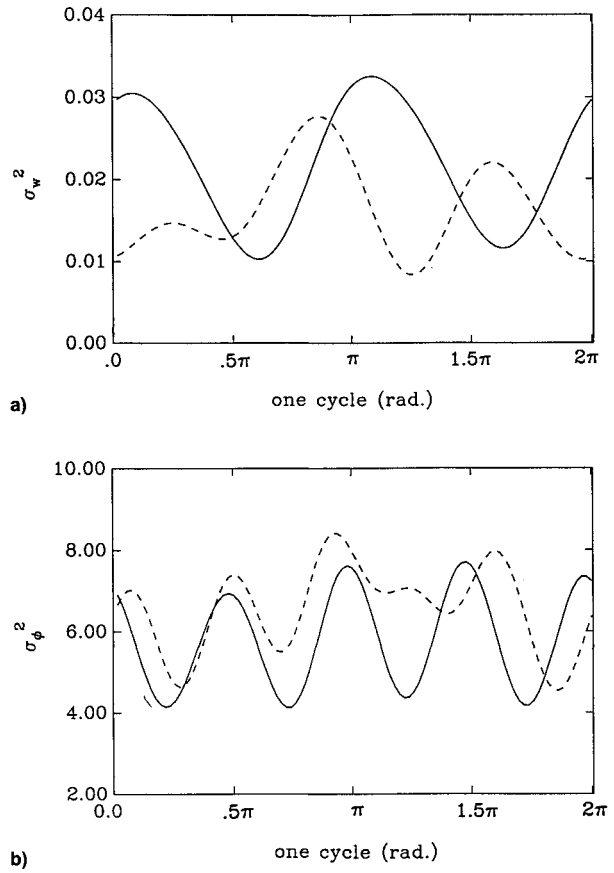

Fig. 8 Comparison between two computational methods for the variance response; - -, for the direct time domain method; —, for the time-frequency domain method, for a) σ_w^2 vs ψ and b) for σ_ϕ^2 vs ψ.

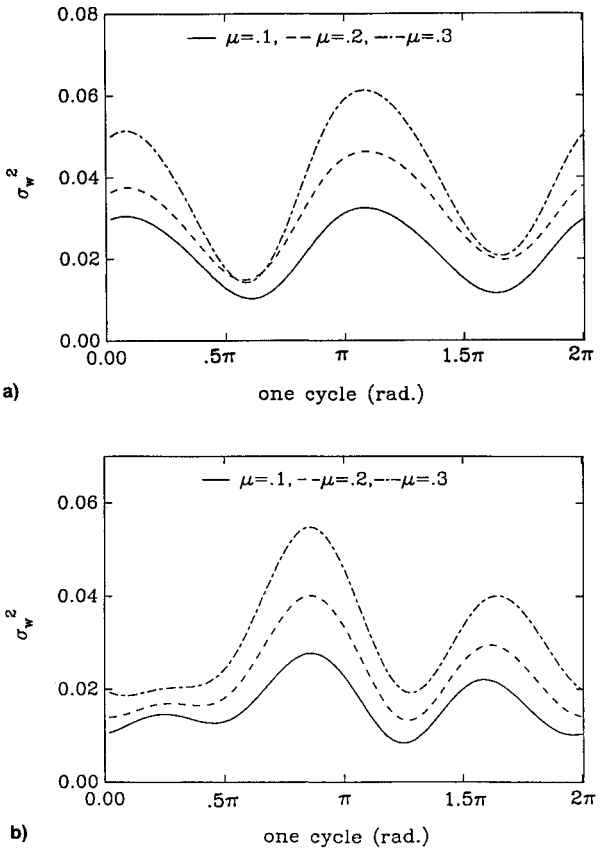

Fig. 9 σ_w^2 vs ψ for $u_0 = 23$ m/s, $\theta_0 = 0$ and $\mu = 0.1, 0.2, 0.3$, for a) time-frequency method and b) for direct time domain method.

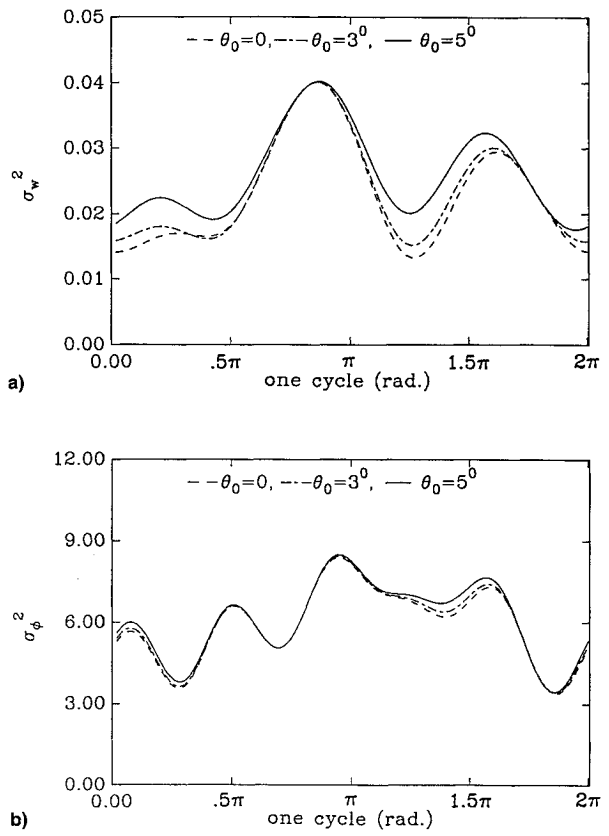

Fig. 10 Variance response vs ψ for u_0 = 23 m/s, μ = 0.2 and θ = 0, 3, 5 deg, for a) σ_w^2 vs ψ and b) for σ_ϕ^2 vs ψ.

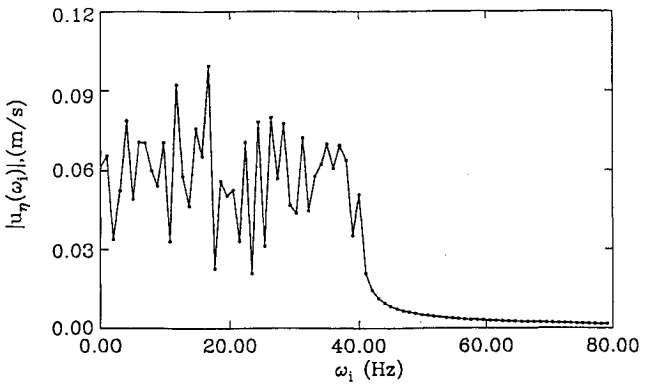

Fig. 11 FFT plot of the longitudinal turbulence.

23 m/s, Ω = 8 Hz, as obtained from the direct time domain method and time-frequency method, respectively. The solid, dashed, and dashed point lines denote μ = 0.1, 0.2, and μ = 0.3, respectively. The amplitudes increase as μ increases. As shown in Fig. 9a, the standard deviation (square-root of the variance) of the flap response reaches a maximum value of 0.16 in. at the tip of blade for μ = 0.1, 0.2 in. for μ = 0.2, and 0.23 in. for μ = 0.3 at approximately $\psi = 0.8\pi$. As μ increases, the azimuth angles corresponding to the maximum and minimal standard deviation response do not change, but for a realistic helicopter rotor in forward flight it does. For the latter, there is a reversed flow region near the blade root when μ increases, which is not modeled in the present analysis. For Fig. 9b, similar results are obtained, but the azimuth angle corresponding to the maximum standard deviation response is near $\psi = \pi$. For both Figs. 9a and 9b, the variance responses are periodic.

Figures 10a and 10b show the time-varying variance responses for the flap and torsional motions for several initial pitch angles θ_0 and μ = 0.2, u_0 = 23 m/s, Ω = 8 Hz as obtained from the direct time domain method. As θ_0 increases

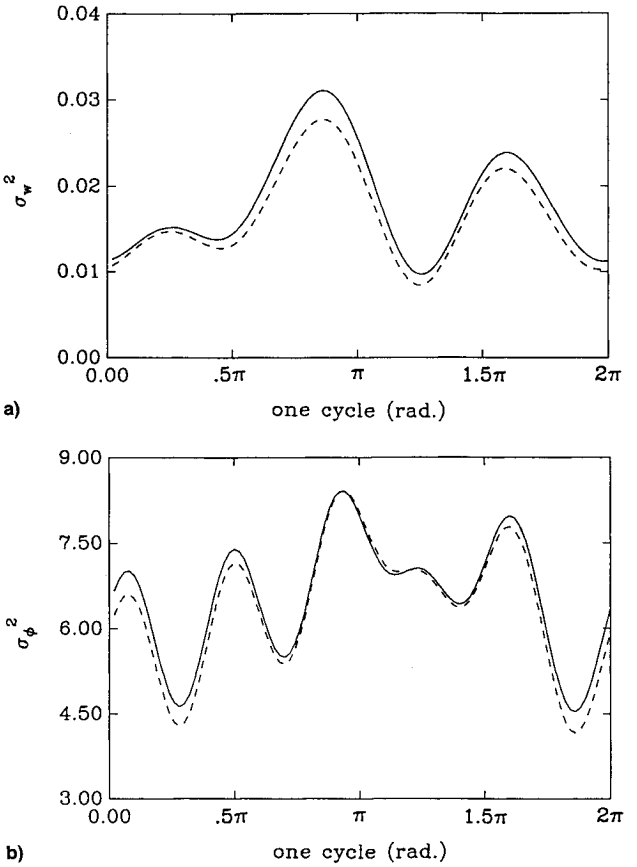

Fig. 12 Comparison between u_η = 0 (- -) and $u_\eta \neq 0$ (—) for the variance response to a lateral gust excitation using the time direct domain method, for a) σ_w^2 vs ψ and b) for σ_ϕ^2 vs ψ.

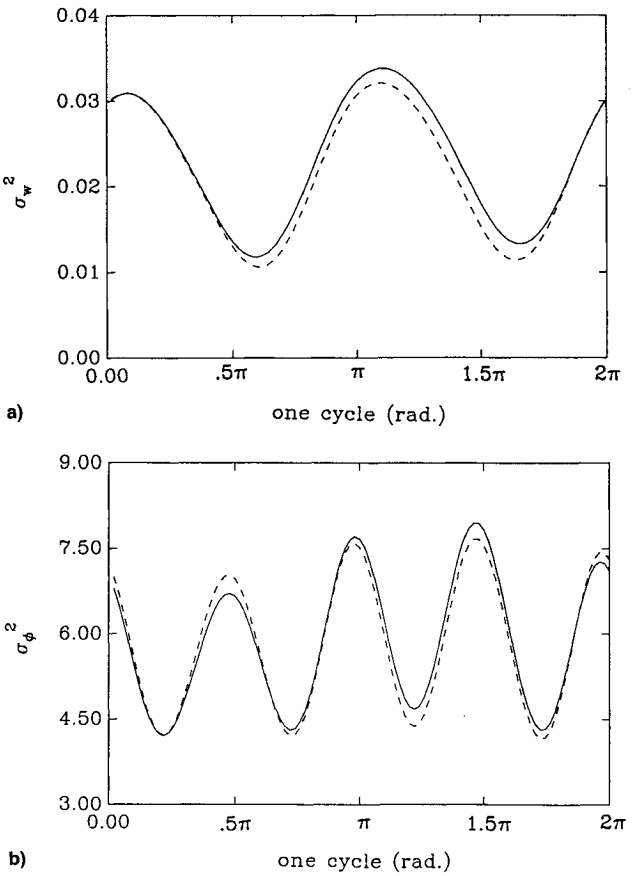

Fig. 13 Comparison between u_η = 0 (- -) and $u_\eta \neq 0$ (—) for the variance response to a lateral gust excitation using the time-frequency domain method, for a) σ_w^2 vs ψ and b) σ_ϕ^2 vs ψ.

from 0 to 5 deg, the flap variance response increases, but does not significantly change as shown in Fig. 10a. For the torsional variance response, the variation is very slight as θ_0 increases as shown in Fig. 10b. This is because the present system model is linear. The influence of the higher harmonic aerodynamic forces due to the sinusoidal pulsating flow is small when θ_0 increases.

B. Random Parametric Excitation

In this case, the longitudinal gust velocity includes both the sinusoidal pulsating stream component and the turbulence component. The turbulence amplitude u_η/u_0 and frequency band are about 0.2 μ and 0–40 Hz, respectively. Shinozuka's algorithm[17] is used to calculate the turbulence process as a periodic series in the time-frequency method. The results are represented as a FFT plot of the turbulence as shown in Fig. 11. In the algorithm $N = 100$, and the frequency varies from 0 to 80 Hz. For the direct time domain method, the theoretical time histories of the lateral and longitudinal gust are used. The results are shown in Figs. 12 and 13 for $u_0 = 23$ m/s, $\mu = 0.1$, $\theta_0 = 0$ deg, and the same gust excitation as in the above example. Figure 12 shows the results obtained from the direct time domain method, and Fig. 13 from the time-frequency method. Figures 12a and 13a are for the flap variance response, and Figs. 12b and 13b are for torsional response. For comparison, the results from the nonrandom parametric excitation (dashed line) are also plotted in Figs. 12 and 13. It is found that due to the random component of the parametric excitation, both the flap and torsional variance responses are greater than the variance responses previously obtained for nonrandom parametric excitation. The increased magnitude of these responses depends upon the amplitude of the longitudinal turbulence. In the present example, the effect of the random parametric excitation on the variance response is shown to not be very significant.

V. Concluding Remarks

Classical and linear ONERA aerodynamic models are applied using time-frequency and direct time domain computational methods, respectively, to calculate the variance gust responses of a nonrotating rotor blade model in a longitudinal sinusoidal pulsating flow. The numerical calculations indicate that the statistically quantitative agreement for both flap and torsional variance responses between the linear ONERA and classical aerodynamic models is reasonably good.

The variance responses depend upon many factors, the sinusoidal pulsating amplitude, gust strength and frequency bandwidth, and the initial pitch angle of the blade. Most significant is the sinusoidal pulsating amplitude. The random parametric excitation due to the longitudinal turbulence component increases the variance responses for both the flapping and torsional motions. However, the effect is not significant for the examples studied here.

The modified linear ONERA aerodynamic model is convenient for use in the direct time domain method. The gust response calculations using this aerodynamic model are in reasonable agreement with experimental results as shown in the companion article, Part II.[24]

Acknowledgments

This work was supported by the Army Research Office under Grant DAAL03-87-K-0023, Gary Anderson is the technical monitor. All numerical simulations were done on the supercomputer, Cray Y-MP, in the North Carolina Supercomputing Center (NCSC), Research Triangle Park, North Carolina.

References

[1]George, V. V., Gaonkar, G. H., Prasad, J. V. R., and Schrage, D. P., "On the Adequacy of Modeling Turbulence and Related Effects on Helicopter Response," *AIAA Journal*, Vol. 30, No. 6, 1992, pp. 1468–1479.

[2]Papoulis, W., *Probability, Random Variable and Stochastic Processes*, McGraw-Hill, New York, 1984, Chap. 9.

[3]Bir, G. S., and Chopra, I., "Gust Response of Hingeless Rotors," *Journal of the American Helicopter Society*, Vol. 31, April 1986, pp. 33–46.

[4]Prussing, J. E., and Lin, Y. K., "Rotor Blade Flap-Lag Stability in Turbulent Flows," *Journal of the American Helicopter Society*, Vol. 27, No. 2, 1982, pp. 51–57.

[5]Prussing, J. E., and Lin, Y. K., "A Closed-Form Analysis of Rotor Blade Flap-Lag Stability in Hover and Low-Speed Forward Flight in Turbulent Flows," *Journal of the American Helicopter Society*, Vol. 28, No. 3, 1983, pp. 42–46.

[6]Prussing, J. E., Lin, Y. K., and Shiau, T. N., "Rotor Blade Flap-Lag Stability and Response in Forward Flight in Turbulent Flows," *Journal of the American Helicopter Society*, Vol. 29, No. 4, 1984, pp. 81–87.

[7]Fuh, J. S., Hong, C. Y. R., Lin, Y. K., and Prussing, J. E., "Coupled Flap-Torsional Response of a Rotor Blade in Forward Flight Due to Atmospheric Turbulence Excitations," *Journal of the American Helicopter Society*, Vol. 28, No. 3, 1983, pp. 3–12.

[8]Lin, Y. K., Fujimori, Y., and Ariaratnam, S. T., "Rotor Blade Stability in Turbulent Flows-Part I," *AIAA Journal*, Vol. 17, No. 6, 1979, pp. 545–552.

[9]Lin, Y. K., Fujimori, Y., and Ariaratnam, S. T., "Rotor Blade Stability in Turbulent Flows-Part II," *AIAA Journal*, Vol. 17, No. 7, 1979, pp. 673–678.

[10]Gaonkar, G. H., "Gust Response of Rotor and Propeller System," *Journal of Aircraft*, Vol. 18, No. 5. 1981, pp. 389–396.

[11]Gaonkar, G. H., and Hohenemser, K. H., "Stochastic Properties of Turbulence Excited Rotor Blade Vibrations," *AIAA Journal*, Vol. 9, No. 3, 1971, pp. 419–424.

[12]Gaonkar, G. H., Hohenemser, K. H., and Yin, S. K., "Random Gust Response Statistics for Coupled Torsion-Flapping Rotor Blade Vibrations," *Journal of Aircraft*, Vol. 9, No. 10, 1972, pp. 726–729.

[13]Gaonkar, G. H., and Hohenemser, K. H., "An Advanced Stochastic Model for Threshold Crossing Studies of Rotor Blade Vibrations," *AIAA Journal*, Vol. 10, No. 8, 1972, pp. 1100, 1101.

[14]Riaz, J., Prasad, J. V. R., Schrage, D. P., and Gaonkar, G. H., "Atmospheric Turbulence Simulation for Rotorcraft Applications," *Journal of the American Helicopter Society*, Vol. 38, No. 1, 1993, pp. 84–88.

[15]Costello, M., Gaonkar, G. H., Prasad, J. V. R., and Schrage, D. P., "Some Issues on Modeling Atmospheric Turbulence Experienced by Helicopter Rotor Blades," *Journal of the American Helicopter Society*, Vol. 37, No. 2. 1992, pp. 71–75.

[16]Greenberg, J. M., "Airfoil in Sinusoidal Motion in a Pulsating Stream," NACA TN 1326, June 1947.

[17]Shinozuka, M., and Jan, C. M., "Digital Simulation of Random Processes and Its Applications," *Journal of Sound and Vibration*, Vol. 25, No. 1, 1972, pp. 111–128.

[18]Petot, D., "Differential Equation Modeling of Dynamic Stall," *Recherche Aerospatiale*, Vol. 5, No. 5, 1989, pp. 51–64.

[19]Peters, D. A., "Toward a Unified Lift Model for Use in Rotor Blade Stability Analyses," *Journal of the American Helicopter Society*, Vol. 30, No. 2, 1985, pp. 32–42.

[20]Dunn, P., and Dugundji, J., "Nonlinear Stall Flutter and Divergence Analysis of Cantilevered Graphite/Epoxy Wings," *AIAA Journal*, Vol. 30, No. 1, 1992, pp. 153–161.

[21]Fung, Y. C., *An Introduction of the Theory of Aeroelasticity*, Wiley, New York, 1955, pp. 344, 345 and pp. 409–412.

[22]Tang, D. M., and Dowell, E. H., "Experimental and Theoretical Study for Nonlinear Aeroelastic Behavior of a Flexible Rotor Blade," *AIAA Journal*, Vol. 31, No. 6, 1993, pp. 1133–1142.

[23]Laning, J. H., and Battin, R. H., *Random Processes in Automatic Control*, McGraw-Hill, New York, 1956.

[24]Tang, D. M., and Dowell, E. H., "Response of a Nonrotating Rotor Blade to Lateral Turbulence Part II: Experiment," *Journal of Aircraft*, Vol. 32, No. 1, 1995, pp. 154–160.